Blume, T., Krause, S., Meinikmann, K., Lewandowski, J. (2013): Upscaling lacustrine groundwater discharge rates by fiber-optic distributed temperature sensing. - *Water Resources Research*, *49*, 12, p. 7929-7944

DOI: http://doi.org/10.1002/2012WR013215

WATER RESOURCES RESEARCH, VOL. 49, 7929–7944, doi:10.1002/2012WR013215, 2013

Upscaling lacustrine groundwater discharge rates by fiber-optic distributed temperature sensing

Theresa Blume,[1] Stefan Krause,[2] Karin Meinikmann,[3] and Jörg Lewandowski[3]

Received 31 October 2012; revised 28 October 2013; accepted 30 October 2013; published 4 December 2013.

[1] Despite the importance of groundwater inflow for water quantity and quality of many lakes world wide, adequate methodologies for the determination of lacustrine groundwater discharge (LGD) rates at scales larger than the point scale and with sufficient spatial resolution are still lacking. Observations of suitably large data sets for the calculation of groundwater discharge rates by traditional methods are very time and labor intensive, often limiting the spatial extent or resolution of experimental investigations. The present study compares upscaling approaches that utilize information on LGD rates derived from a single transect of either sediment temperature profiles or vertical hydraulic gradients. Two transfer functions that integrate the single-transect information with spatially detailed temperature measurements based on fiber-optic distributed temperature sensing (FO-DTS) were developed and tested for their ability to identify 2-D patterns of LGD rates at larger scales. Results were compared with a simplified approach, based on the pragmatic assumption of exponential decline of LGD rates perpendicular to the shoreline. Both FO-DTS based upscaling approaches were able to reproduce the distinct small-scale heterogeneities in LGD patterns and quantities that were observed in an extensive reference survey using LGD estimates based on sediment temperature profiles. The transfer functions generated satisfactory representations of flow patterns, even when only low numbers (4 in this case) of reference measurements were used for their calibration, thus providing a successful proof of concept for this methodology and encouraging its further application at large scales.

Citation: Blume, T., S. Krause, K. Meinikmann, and J. Lewandowski (2013), Upscaling lacustrine groundwater discharge rates by fiber-optic distributed temperature sensing, *Water Resour. Res.*, *49*, 7929–7944, doi:10.1002/2012WR013215.

1. Introduction

[2] The water balance and chemistry of lakes with little or no surface inflow can be substantially impacted by the spatial pattern of lacustrine groundwater discharge (LGD) and corresponding fluxes of nutrient or pollutant inputs across the groundwater-surface water interface [*Loeb and Goldman*, 1979; *Enell*, 1982]. The quantification of groundwater-borne loads requires the determination of both, water fluxes and concentrations of relevant compounds in groundwater discharge. Due to the spatial heterogeneity of exchange fluxes at the sediment-water interface, the determination of groundwater discharge and its chemical load is often a challenge. This study focuses on the identification and quantification of groundwater discharge and its spatial pattern.

1.1. Spatial Patterns of Seepage Fluxes

[3] Exchange fluxes between groundwater and surface water are controlled (i) by hydraulic head gradients between aquifer and lake as the driving force and (ii) by the spatial distribution of hydraulic conductivity of sediments at the aquifer-lake interface. Spatial variability in drivers (hydraulic head gradients) and controls (hydraulic conductivity) of exchange fluxes determine patterns of lacustrine groundwater discharge (LGD). Significant spatial heterogeneity of seepage fluxes has been revealed by a number of experimental studies [e.g., *Kishel and Gerla*, 2002; *Kidmose et al*., 2011; *Cherkauer and Nader*, 1989; *Lautz and Ribaudo*, 2012]. For example, *Kishel and Gerla* [2002] identified significant horizontal and vertical heterogeneity of flow directions and fluxes within a densely spaced grid of piezometers (every 2 m in a 10 × 10 m domain). *Lautz and Ribaudo* [2012] used flux rates from heat transport modeling based on time series and streambed temperatures to develop an upscaling approach for a 30 m stream reach.

[4] For homogenous isotropic aquifers, LGD has been found to concentrate in a narrow band close to the shore [*McBride and Pfannkuch*, 1975]. As a consequence, shallow groundwater usually discharges close to the shore whereas smaller fluxes of deeper groundwater discharge more offshore [*McBride and Pfannkuch*, 1975; *Frape and Patterson*, 1981]. Increased seepage rates at nearshore

[1]GFZ German Research Centre for Geosciences, Potsdam, Germany.
[2]School of Geography, Earth and Environmental Sciences, University of Birmingham, Birmingham, UK.
[3]Department of Ecohydrology, Leibniz-Institute of Freshwater Ecology and Inland Fisheries, Berlin, Germany.

Corresponding author: T. Blume, GFZ German Research Centre for Geosciences, Telegrafenberg, DE-14473 Potsdam, Germany. (blume@gfz-potsdam.de)

0043-1397/13/10.1002/2012WR013215

areas may also result from the spatial distribution of fine-grained, low-permeability muddy sediments in a lake. The depth of the muddy sediment is usually largest in the central parts of a lake and decreases toward the shore. Wave action can resuspend light, freshly deposited material from shallow areas while material that settled in deeper parts of a lake is less affected. Thus, hydraulic conductivities of shoreline sediments are usually higher than of sediments from deeper lake sections [*Kishel and Gerla*, 2002; *McBride and Pfannkuch*, 1975; *Krabbenhoft et al*., 1990b]. The fact that highest seepage rates usually occur in near vicinity to the shore is convenient for the experimental determination of seepage rates as measurements can be conducted in the shallowest and most accessible parts of the lake. In many lakes, this means that seepage measurements can be conducted by wading, rather than from boats or by diving [*Shaw et al*., 1990].

[5] The spatial patterns of seepage rates in their relation to shore distances have been studied by direct measurements with seepage meters [*Lee*, 1977; *Brock et al*., 1982; *Harvey et al*., 2000] and by the application of numerical models [e.g., *Pfannkuch and Winter*, 1984; *Shaw and Prepas*, 1990; *Schafran and Driscoll*, 1993]. However, the identification of spatial patterns and quantification of seepage fluxes across aquifer-lake interfaces is a major challenge. Quantitative approaches either treated an entire lake as a lumped system, and therefore estimations lacked detailed information on spatial patterns [*Brock et al*., 1982; *Krabbenhoft et al*., 1994; *Harvey et al*., 2000] or were based on point measurements, i.e., point estimates of local fluxes [*Lee*, 1977]. As point observations are representative for the specific local conditions and processes only, a large number of labor-intensive measurements is required and an extrapolation of these observations to the entire lake encompasses high uncertainty. Hence, current studies of lake water balances and nutrient budgets often lack adequate information of spatial patterns of seepage fluxes across the aquifer-lake interface, which critically limits the representativeness of results.

1.2. Quantitative Methods for Estimating Seepage Flow

[6] Recent years have seen the development and application of a wide range of approaches for monitoring and quantifying LGD. Net exchange of groundwater has been estimated by identifying and solving the different components of the water balance equation [*Brock et al*., 1982; *Belanger et al*., 1985; *Harvey et al*., 2000]. Furthermore, mass balances of stable isotopes [*Krabbenhoft et al*., 1994] or conservative chemical tracers such as chloride [*Krabbenhoft and Webster*, 1995] have been used to quantify LGD. However, all mass balance approaches integrated spatial heterogeneities and temporal variability of the flow field and thus, did not provide spatially detailed information of exchange flow patterns [*Krabbenhoft et al*., 1990a].

[7] In contrast to the aforementioned lumped approaches for entire lakes, seepage meters that are deployed at the sediment-water interface for measuring water fluxes over a specified area of the lake bed [*Lee*, 1977; *Kalbus et al*., 2006] provide a possibility for direct monitoring of small-scale exchange fluxes between groundwater and surface water [*Rosenberry*, 2005]. Further indirect methods for quantifying LGD rates are based on Darcy's law and require detailed observations of pressure head gradients (e.g., in piezometers) and hydraulic conductivity of the local aquifer [*Stauffer*, 1985; *Kishel and Gerla*, 2002]. Sediment depth profiles of temperature [*Schmidt et al*., 2006; *Stonestrom and Constantz*, 2003; *Anibas et al*., 2009; *Meinikmann et al*., 2013] or conservative ions [*Mortimer et al*., 1999; *Schuster et al*., 2003] at the sediment-water interface have been successfully analyzed for indirect determination of water fluxes at the groundwater-surface water interface. However, the application of these methods is subject to certain assumptions (see sections 2.2.2 and 4.1) and requires the existence of distinct differences in the respective characteristics of the groundwater and surface water end-members. If end-member characteristics are distinctive, fluxes can be calculated from the curvature of the observed gradient at the sediment-water interface. Dampening and phase shifts of diurnal temperature oscillations can be used if time series of temperature profiles are available [e.g., *Hatch et al*., 2006, *Constanz*, 2008]. Despite some problems in using temperature as a tracer arising from diurnal signal propagation during snapshot sampling or retardation effects (since temperature is not a conservative tracer) these methods have been successfully applied for the quantification of 1-D vertical fluxes at the groundwater-stream interface [*Hatch et al*., 2006; *Hannah et al*., 2009; *Krause et al*., 2011; *Meinikmann et al*., 2013].

1.3. Fiber-Optic Temperature Sensing

[8] Recent developments in fiber-optical sensor technologies provide a novel and robust methodology for investigating spatial patterns of exchange fluxes between groundwater and surface water by Fiber-Optic Distributed Temperature Sensing (FO-DTS) [*Selker et al*., 2006a, 2006b; *Tyler et al*., 2009; *Krause et al*., 2012]. Based on the differences in groundwater and surface water temperatures, spatial patterns of groundwater discharge can be identified by tracing temperature anomalies at the sediment-water interface. Temperatures can be traced along fiber-optic cables of several kilometers length with currently 0.3–4 m spatial resolution and measurement precision of 0.05–0.1°C for sampling intervals of 30 s [*Selker et al*., 2006a; *Hausner et al*., 2011; *Van de Giesen et al*., 2012]. In contrast to the aforementioned methodologies, FO-DTS is useful for spatially detailed measurements at larger scales, and therefore has the potential to provide temperature information for tracing LGD with high spatial resolution at scales exceeding previous detailed investigations of local flow. FO-DTS has successfully been applied for qualitative identification of complex of groundwater upwelling patterns in streams [*Slater et al*., 2010; *Mwakanyamale et al*., 2012], wetlands [*Lowry et al*., 2007], and coastal zones [*Henderson et al*., 2009]. Hence, spatially detailed FO-DTS observations may provide an adequate measure to upscale detailed point observations or provide an efficient screening tool for identifying locations for detailed analyses of groundwater upwelling. The upscaling approach based on DTS data described in this study is novel as here DTS data are related to lacustrine groundwater discharge determined by both temperature profile gradients and vertical hydraulic gradients and thus allows for the quantification of flux rates. This is an important

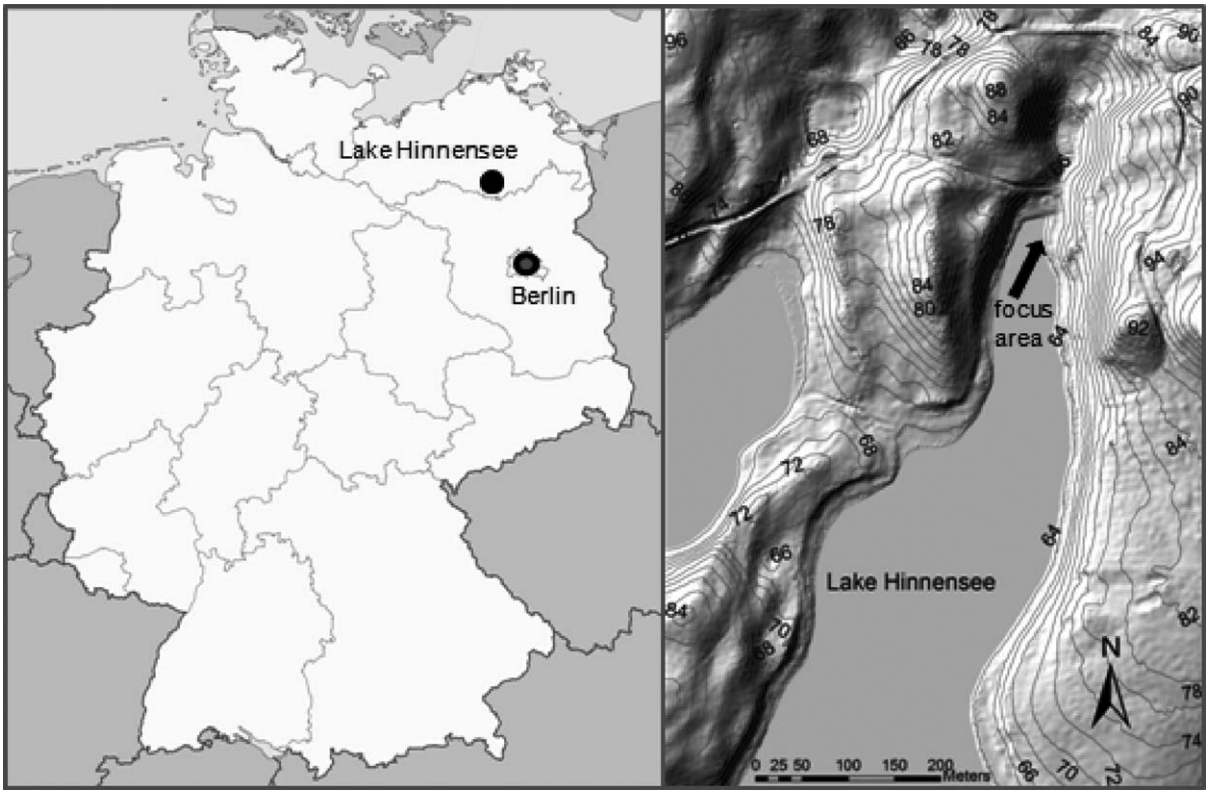

Figure 1. Location of Lake Hinnensee and the focus area.

improvement of DTS application beyond simply visualizing the spatial pattern of groundwater discharge.

1.4. Objectives

[9] The objective of the present study is to test whether FO-DTS-based upscaling of point measurements of lacustrine groundwater discharge rates is an adequate and feasible approach to represent the spatial heterogeneity of LGD rates. A transect of piezometers for determination of vertical hydraulic gradients is therefore combined with a manually measured grid of vertical temperature profiles and a FO-DTS survey of temperatures at the lake-aquifer interface. Obtaining a large data set of temperature profiles or vertical hydraulic gradients (VHG) is time consuming and tedious and hence often limits the spatial extent and resolution of experimental studies. We therefore derived and tested two upscaling methodologies based on information from a single transect of either temperature profile or VHG-derived LGD estimations. The two transfer functions combined this information with FO-DTS temperature measurements to identify detailed 2-D patterns of LGD rates at a larger scale. These DTS-based upscaling approaches were compared to a very simple 1-D-upscaling approach based on the assumption of exponential decline of LGD with distance to the shore.

2. Material and Methods

2.1. Research Area: Lake Hinnensee

[10] Lacustrine groundwater discharge (LGD) was investigated at a shore section of Lake Hinnensee, a groundwater dominated lake located in the north-eastern lowlands of Germany in the Mueritz National Park (Figure 1). The landscape has been shaped by glacial and postglacial processes of the Weichsel glaciations and Lake Hinnensee was formed in a glacio-fluvial tunnel valley. The lake covers an area of 49 ha and has a maximum depth of 14 m (on average 7 m). At the southern end Lake Hinnensee is connected to Lake Fürstensee. The northern catchment boundary is constituted by a terminal moraine which coincides with the North Sea/Baltic Sea groundwater divide. However, most of the catchment is located in the outwash plain and soils are generally sandy. Elevations of the catchment range from 63 to 124 m above sea level. The majority of the catchment area is covered by forest with predominantly beech, pine and oak species. The lake is mesotrophic.

[11] The climate of the area is continental; mean annual rainfall recorded in Neustrelitz (10 km northwest of Lake Hinnensee) amounts to 610 mm (1901–2005, DWD-German Weather Service) and mean annual temperature is 8.1°C (1901–2005, DWD-German Weather Service).

[12] The experimental investigations of this study focussed on a 20 m long shore section at the northern tip of Lake Hinnensee (Figures 1 and 2). The land side of the study site is characterized by a margin of moderate slopes which become steeper with greater distance to the lake. The lake sediment of the study site is predominantly composed of fine and medium sand with some organic materials like branches, roots, and leaves. The southern end of the field site is covered by reeds. The topography of the lake bed at the field site is characterized by gentle slopes developing into steeper gradients at approximately 2–3 m

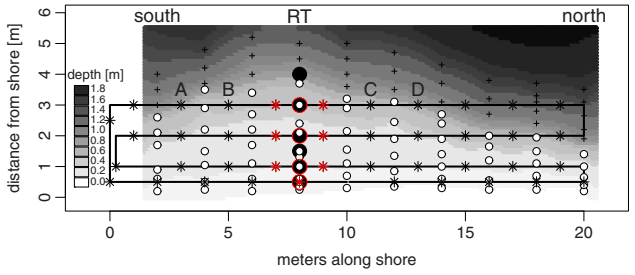

Figure 2. Experimental layout: Lake bathymetry along the investigated shoreline. White circles indicate locations where sediment temperature profiles and water depth were measured, black crosses show locations where only water depth was surveyed and black circles mark the locations of piezometers. The transect where the piezometers are located is called the reference transect (RT). The black line indicates the positioning of the fiber-optic cable and the stars mark the DTS sampling locations (note that DTS data is integrated over 4 m with the DTS system used here). The sediment core was taken at 1 m distance from shore at the reference transect (RT). Data points used for the final transfer functions are plotted in red while the other transects are indicated by the letters A to D.

distance to the shore (Figure 2). The lake bed topography was surveyed along 10 transects perpendicular to the shoreline reaching 3–5 m into the lake.

2.2. Experimental Design

[13] The heterogeneity and patterns of groundwater-surface water interactions at the shore section were investigated by three different methods: (a) a transect of piezometers to determine vertical hydraulic gradients, (b) sediment temperature depth profiles measured manually with a temperature probe along a grid, and (c) temperature measurements along a fiber-optic cable (FO-DTS) deployed at the lake bed surface (Figure 2).

2.2.1. Vertical Hydraulic Head Gradients at Piezometers and Determination of LGD Rates

[14] Vertical hydraulic gradients (VHG), indicating the strength and direction of exchange fluxes between groundwater and lake, were determined from hydraulic head measurements along a transect of nearshore piezometers. Polyvinyl chloride (PVC) piezometers of 32 mm inner diameter and a 10 cm bottom screening section were installed within the lake sediments to depths of 50, 100, and 150 cm at 0.5, 1.0, 1.5, 2.0, 2.5, and 3.5 m distance to the shoreline (reference transect RT, Figure 2). Hydraulic heads in the piezometers were monitored manually on 15 September 2010 and 16 September 2010 using a graduated electric contact meter (dip-meter). Based on Δh, the elevation difference of the groundwater observed inside and the lake water table outside the piezometer and Δl given by the distance between the midscreen depth and the sediment-water interface, VHG were calculated by $\Delta h/\Delta l$. The accuracy of dip-meter-based hydraulic head observations was approximately ± 2 mm head and accounts for uncertainties in the measurements introduced by small wind-induced waves around the piezometers, which can affect the outside head estimates but are assumed to be smaller than in river environments with turbulent flow [*Krause et al*., 2009; *Kaeser et al*., 2009], especially as wind velocities were low during the measurements (1 m/s on average). The hydraulic conductivity of the lake sediment was estimated using four different methodologies. A 108 cm long sediment core was taken at 1 m distance from the shore at the piezometer transect (see Figure 2). The core was split into 11 samples of approximately 10 cm length and grain size distributions were determined in the lab. In order to obtain hydraulic conductivities, these grain size distributions were used as input for the pedotransfer function model Rosetta (United States Salinity Laboratory, release date 1999, http://www.ars.usda.gov/Services/docs.htm?docid=8953) and the Hazen approximation $Ks = 0.0116 * d_{10}^2$, with Ks being the hydraulic conductivity in m/s and d_{10} being the grain size diameter that bounds the lowest 10% percentile of the sample in µm. For both methods, Ks was determined for each sample individually and then was averaged over the profile using the geometric mean. These results were compared to the Ks value determined with the Hvorslev method based on pump test data from a piezometer at the field site at 1.8 m distance from shore (pump test carried out in 2012). Finally, Ks was also inferred as a result of an optimization by fitting the VHG-based exfiltration rates to the temperature profile-based exfiltration rates at the same locations.

[15] LGD rates were calculated using the observed vertical hydraulic gradients and the estimated hydraulic conductivities:

$$LGD_{\text{rate}} = Ks \times A \times VHG \times 1000 \quad (1)$$

[16] With LGD_{rate} in $L/m^2/d$, Ks being the mean hydraulic conductivity in m/d, and A the unit area in m^2. Vertical hydraulic gradients (VHG) are given in m/m.

2.2.2. Depth Profiles of Sediment Temperatures to Determine LGD Rates

[17] Temperature depth profiles of the lake sediment were measured from 14th to 16th September (two thirds of the profiles on 15th September) with a high-precision digital thermometer (Greisinger GMH 3750) equipped with a needle thermocouple (Greisinger GES 401, needle of 45 cm length and 3 mm diameter, sensor element Pt100 in the tip of the needle, accuracy ± 0.03°C). The needle was inserted several centimeters deep into the sediment and after reaching a constant temperature, sediment depth and temperature were recorded. Usually, constant temperature values were reached within less than 2 min. Afterward, the needle was pushed deeper into the sediment. That procedure was repeated until reaching the maximum penetration depth of the needle which was limited to 45 cm. At five locations, reaching the maximum depth was prevented by obstacles (stones, roots) in 35 to 45 cm depth. Usually surface water temperature and temperatures at six or seven depths were recorded for each depth profile. Depth profiles were measured along a gridded design with 10 transects from the shore into the lake (see Figure 2). Transects were spaced 2 m apart. The extent of the transects into the lake depended on the local bathymetry and was limited by the requirement to reach the lake bottom for probe injection. Thus, transects varied in length between 1 and 4 m. The reference transect (RT) was measured both on 14th and 15th September. Surface water temperature during the 3

days of the measurement campaign varied from 16.1 to 17.3°C.

[18] For calculating LGD rates based on depth profiles of sediment temperature, the procedure described by *Schmidt et al*. [2006] was followed. With the assumption that groundwater flow in the sediment is vertical, the governing equation for 1-D conductive and advective heat transport is

$$K_{fs}\frac{\partial^2 T(z)}{\partial z^2}-q_z\rho_f c_f\frac{\partial T(z)}{\partial z}=\rho c\frac{\partial T(z)}{\partial t} \quad (2)$$

[19] Where: K_{fs} (J s^{-1} m^{-1} K^{-1}) is the thermal conductivity of the saturated sediment; $T(z)$ (°C) is the streambed temperature at depth z; q_z is the vertical flux (m s^{-1}); $\rho_f c_f$ (J m^{-3} K^{-1}) is the volumetric heat capacity of the fluid; ρc (J m^{-3} K^{-1}) is the volumetric heat capacity of the saturated sediment; and t is the time (s).

[20] A further prerequisite for the application of the method using temperature depth profiles is the assumption that the system is at steady state. Under this condition, the term right of the equal sign of equation (2) is zero [*Anibas et al*., 2009]. *Bredehoeft and Papadopulos* [1965] presented an analytical solution for this case given in equation (3).

$$T(z)=\frac{\exp\left(\frac{q_z\rho_f c_f}{K_{fs}}z\right)-1}{\exp\left(\frac{q_z\rho_f c_f}{K_{fs}}L\right)-1}(T_L-T_0)+T_0 \quad (3)$$

[21] Where: L (m) is the depth of the lower boundary, i.e., the thickness of the zone in which vertical changes of the temperature occur due to temperature differences between groundwater and lake water; T_0 (°C) and T_L (°C) are the constant temperatures at the upper (surface water) and lower (groundwater) boundaries, respectively.

[22] The temperature of the lower boundary T_L was estimated as 11°C based on measurements in the 1–1.5 m deep piezometers close to the shoreline. 11°C seems a plausible value for the near-surface aquifer underneath a forest. The value for the volumetric heat capacity $\rho_f c_f$ of the water ($4.19 * 10^6$ J m^{-3} K^{-1}) was obtained from literature. Values for the thermal conductivity K_{fs} of saturated sediments have a much smaller range (1.4–2.2 J s^{-1} m^{-1}°C^{-1}) than the hydraulic conductivity and are almost independent of sediment texture [*Stonestrom and Constantz*, 2003]. The thermal conductivity K_{fs} of Lake Hinnensee sediment was not measured within this study but based on values reported by *Stonestrom and Constantz* [2003] was estimated to be 2 J s^{-1} m^{-1}°C^{-1}.

[23] The flux q_z was estimated by fitting the analytical solution of the heat transport equation (using the Microsoft Office Excel 2003 Solver) for each temperature depth profile so that the root mean squared error (RMSE) between measured temperatures $T_{meas}(z)$ and the ones modeled based on equation (2) was minimal for the profiles consisting of m points:

$$RMSE=\sqrt{\frac{1}{m}\sum_{j=1}^{m}\left(T_{meas}(z_j)-T(z_j)\right)^2} \quad (4)$$

[24] The calculation of the *RMSE* (equation (4)) requires *T(z)* to be calculated which furthermore requires information on the interface thickness L (equation (3)). For every depth profile, 34 different values for L ranging from 0.5 to 10 m (with 0.1 m intervals between 0.5 and 2.6 m and then gradually larger spacing) were tested in order to establish the impact of a change of L on q_z and on the quality of the fit. To determine the optimal interface thickness L, we calculated for each L the arithmetic mean of the *RMSE*s of all 67 temperature depth profiles and determined for which L the minimum of the arithmetic mean of the *RMSE*s was reached.

2.2.3. Distributed Fiber-Optic Temperature Sensing (FO-DTS)

[25] Fiber-optic Distributed Temperature Sensing (FO-DTS) was used to investigate temperature patterns at the sediment-water interface as this pattern can be strongly linked to patterns in LGD. FO-DTS uses the temperature-dependent backscatter properties of a laser signal that propagates through a fiber-optic cable [*Selker et al*., 2006a, b; *Tyler et al*., 2009]. The FO-DTS method applied in this project analyses the offset in the backscatter of Raman Stokes (temperature independent) and anti-Stokes (temperature dependent) signals from a 10 ns light pulse to undertake and locate temperature measurements along the fiber-optic cable [*Selker et al*., 2006a, b]. The applied DTS system (Sensornet Halo) is capable of measuring temperature at high precision (0.05°C) with a sampling resolution of 2 m [*Sensornet*, 2009] and a spatial resolution of 4 m [*Van de Giesen et al*., 2012]. For the temperature survey, a gel-coated, plastic covered two channel fiber-optic cable (Bru-Pro, Brugg/CH) was deployed at the sediment surface (ensured by carefully inspecting cable position during installation) in a setup of four parallel loops with 0.5, 1, 2, and 3 m distance to the shoreline (Figure 2). Good contact to the sediment is essential as floating cables will measure lake water temperature only.

[26] DTS measurements were carried out on 15th September. A single-ended measurement setup was deployed with alternating sampling directions that applied the laser pulse to different ends of the fiber-optic cable. Measurements were taken for 30 s intervals in each direction. As one direction showed much less noise than the other, only these traces were averaged (average over 20 traces resulting in a 20 min temporal average). In order to calculate temperature offset and losses along the cable, sections of both cable ends were calibrated in temperature controlled warm/cold baths covering length sections 8–10 times the sampling resolution. Control bath temperatures determined by the DTS measurements after calibration reproduced the temperatures measured with the handheld temperature probe with an RMSE of 0.029, 0.028, 0.050, and 0.102°C for the four calibration sections. The effect of solar radiation on cable temperature is likely to be of minor importance for this study, as the shoreline is well shaded by trees (with even more pronounced shading during the first half of the day when the cable was installed and measurements were carried out). Furthermore, the days of the study were cloudy to partially cloudy and quite cool.

2.2.4. Upscaling LGD Rates: From Single Transect to Shore Section

[27] The potential of upscaling single-transect measurements of LGD to the entire shore section was investigated with three different methodologies: (a) a transfer function

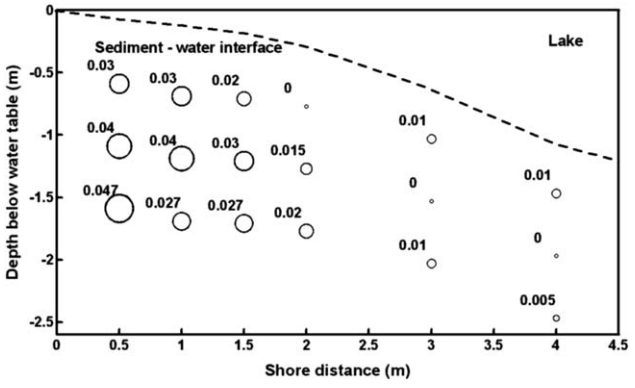

Figure 3. Vertical hydraulic gradients at the piezometer transect (RT).

upscaling temperature profile-based LGD rates by using DTS temperatures, (b) a transfer function upscaling VHG-based LGD rates by using DTS temperatures, and (c) a simple exponential decline function fitted to the reference transect of temperature profile-based LGD rates. All data used for the development for the three transfer functions stemmed from the reference transect (RT) where measurements of both VHG and temperature profiles were available. The interpolated surface of LGD rates based on the entire data set of temperature profiles was used for the purpose of comparison and model evaluation.

[28] In case a and b, a simple regression was carried out to obtain the transfer function. Based on the data set from the temperature profiles, three different model types were investigated for their suitability: linear, exponential and quadratic. This was done using the entire data set, for half the data set and for five different single transects: transects A–D and the reference transect (RT) (for locations see Figure 2). As only one of the DTS sample points is located directly at the reference transect (RT), the DTS measurements to the left and right of the reference transect were simply averaged to obtain paired values of DTS temperatures and LGD rates based either on VHGs or temperature profiles ($n = 4$). The exponential function of case c is based on 12 values of LGD derived from sediment temperature depth profiles and was fitted using Microsoft Excel Solver. Model/upscaling performance was evaluated using RMSE, sum of residuals and comparing the median, mean, minimum and maximum LGD rates of the predicted data set versus the LGD rates determined from the temperature profiles. Note that the LGD rates based on temperature profiles are also not a direct measurement and subject to a number of assumptions (see sections 2.2.2 and 4.1). Unless otherwise indicated data analysis was carried out with the statistical computing software R.

3. Results

3.1. Vertical Hydraulic Gradients

[29] Observations of VHGs along the piezometer transect installed into the lake sediment revealed positive values throughout (Figure 3), ranging from 0 to 0.047. VHGs varied strongly horizontally along the piezometer transect and slightly for different observation depths. VHGs steadily declined with increasing distance to the shore (Figure 3). LGD rates were determined using the vertical hydraulic gradients for 1.5 m depth and the estimated Ks value as input to equation (1). VHGs from this depth were chosen as they showed a similar decline with distance to shore as the LGD rates determined from temperature profiles. VHG uncertainty at this depth is much smaller compared to the shallower depth (the smaller Δh, the larger the effect of the error of ± 2 mm). Hydraulic conductivities Ks estimated by both the pedotransfer function model Rosetta and the Hazen approximation were based on the grain size distributions of the sediment core samples summarized in Table 1. Ks values ranged from 1.4 to $1.6 * 10^{-4}$ m/s with a geometric mean of $1.53 * 10^{-4}$ m/s for the Rosetta model and from 0.5 to $1.8 * 10^{-4}$ m/s with a geometric mean of $0.6 * 10^{-4}$ m/s for the Hazen approximation. However, both the pump test analysis using the Hvorslev method as well as the optimization of Ks based on fitting VHG exfiltration rates to the exfiltration rates determined from temperature profiles resulted in lower Ks with values of $2.45 * 10^{-5}$m/s for the pump test and $3.1 * 10^{-5}$m/s for the optimization. The optimized Ks is quite close to Ks determined from the single-pump test (a more reliable method compared to the approximations based on grain sizes as it is carried out in situ). As the optimized Ks is furthermore based on four data points instead of a single measurement the optimized value was chosen for the determination of LGD rates. Based on this Ks and the VHGs, the LGD rates ranged from 27 L m^{-2} d^{-1} at 3 m, 55 L m^{-2} d^{-1} at 2 m, 73 L m^{-2} d^{-1} at 1 m, and 128 L m^{-2} d^{-1} at 0.5 m distance to the shore (Figure 7c).

3.2. Temperature Depth Profiles

3.2.1. Temperature Patterns

[30] Surface water temperature varied from 16.1 to 17.3°C during the 3 days of the measurement campaign, while groundwater temperature was constant with approximately 11°C.

[31] The entire data set of manual measurements in combination with the corresponding depths below the water table is shown in Figure 4. Transects are plotted starting from the south (to the left) of the shore section. Lowest temperatures were measured at the deepest parts of the profiles in the first meter closest to the shore. This is found to be less pronounced in both of the most southern and northern transects. No clear relationship between temperature patterns and bathymetry could be identified. However, a strong increase of temperatures with increasing distance to

Table 1. Mean Grain Size Distribution Including Standard Deviations Obtained From the Sediment Core Taken at the Investigated Shore Section[a]

Grain Size (μm)	%	Standard Deviation
>2000	5.6	2.2
>1000	5.3	2.2
>500	14.3	6.4
>250	38.6	11.6
>125	29.3	9.8
>63	6.3	4.5
>32	0.3	0.2
<32	0.4	0.2

[a]Values are averaged over the 11 samples taken every 10 cm along the core.

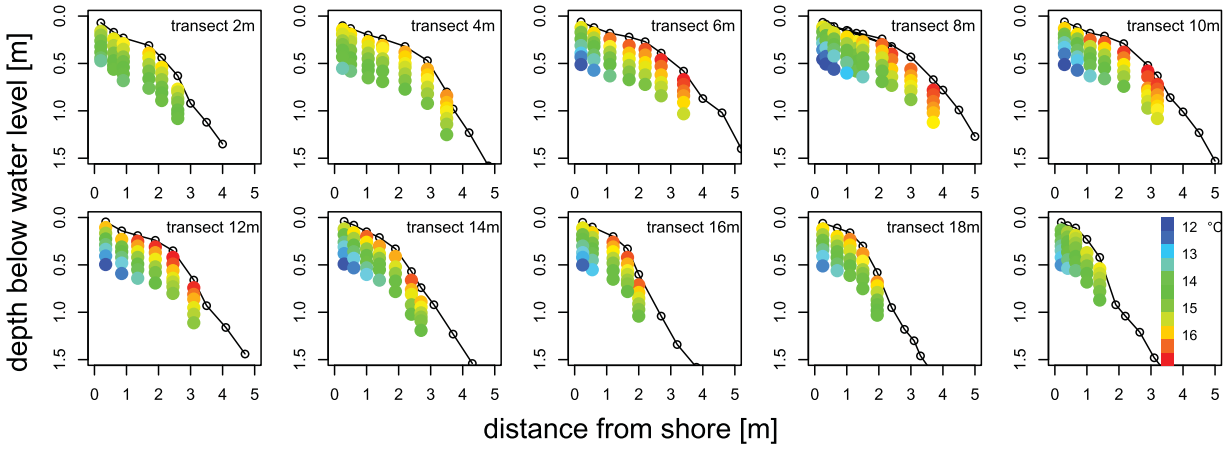

Figure 4. Transects of depth profiles of temperatures along the investigated shore section from south to north including the corresponding bathymetry (black line). Open circles indicate positions where the water depth was measured but no temperature depth profiles were recorded.

the shoreline (exemplary for one depth in Figure 5) was found for all sediment depths.

3.2.2. Determination of LGD Rates From Temperature Profiles

[32] For each vertical temperature profile the flux q_z was calculated based on the solution to the heat transport equation (equation (3)) by minimizing the root mean squared error (RMSE) between measured and simulated temperature profiles (equation (4)). Simulated temperature depth profiles generally fit the measured temperature depth profiles well (RMSE: minimum 0.021°C, arithmetic mean 0.082°C, 90% quantil 0.132°C, maximum 0.187°C, $n = 67$) as can be seen for five examples in Figure 6. The model sensitivity to different interface thicknesses L was tested using the approach described in section 2.2.2. Based on the analysis of all 67 depth profiles, an interface thickness L of 2 m resulted in the lowest *RMSE*. In result, q_z appeared to be independent of L for L larger than a certain threshold (specific to each depth profile), i.e., the resulting fluxes were not influenced by L as long as L was chosen large enough to extend into the zone of spatially constant groundwater temperature. At Lake Hinnensee, LGD rates were found to be essentially independent of L at interface thicknesses $L > 2$ m with a slight optimum at $L = 2$m. This agreed with the findings of *Schmidt et al*. [2006], while Jensen and Engesgaard simply assumed an L of 5 m for their study [*Jensen and Engesgaard*, 2011].

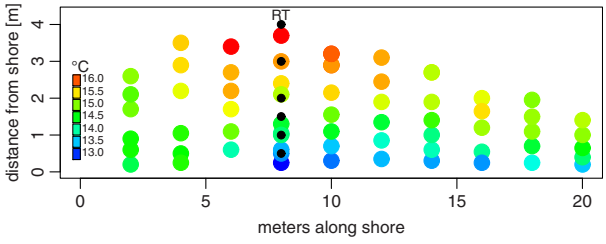

Figure 5. Exemplary temperature pattern along the shore section at a specific depth in the sediment, here for the depth of 26−32 cm. Black circles indicate the location of the piezometers and the reference transect (RT).

[33] LGD rates determined by fitting the heat transport equation to the temperature profiles generally showed a rapid decrease with distance to shore (Figure 7), similar to the LGD rates determined using VHGs (Figure 7c). The maximum LGD rate was found in 25 cm distance to the shore with 169 L m^{-2} d^{-1} at the reference transect (RT) (Figure 7). For the neighboring transects (at 6 −16 m), maximum LGD rates of 129–157 L m^{-2} d^{-1} were found at 20–35 cm distance to the shore (Figure 7b). LGD rates at greater distances to the shore dropped to almost zero. It was found that LGD rates (q_z) decreased exponentially:

$$q_z(d_s) = a \cdot e^{-bd_s} \tag{5}$$

[34] Where d_s is the distance to the shore and a and b are fitting parameters.

[35] Parameters a and b were estimated with the Microsoft Office Excel 2003 Solver based on all q_z estimates of a transect so that the root mean squared error (RMSE)

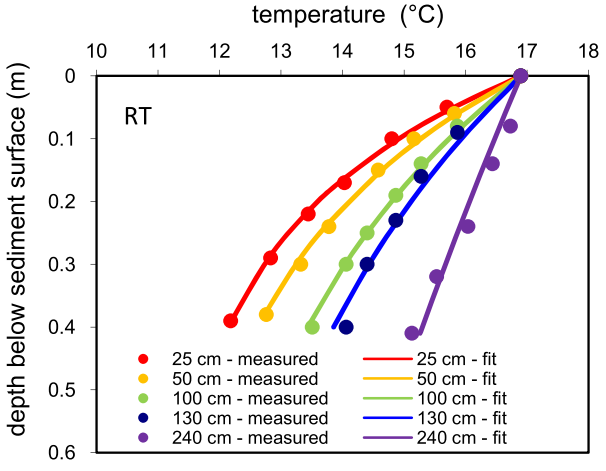

Figure 6. Comparison of measured and simulated depth profiles of sediment temperature based on the heat transport equation. Distance from shore increases from 25 to 240 cm. Examples shown here are from the reference transect (RT).

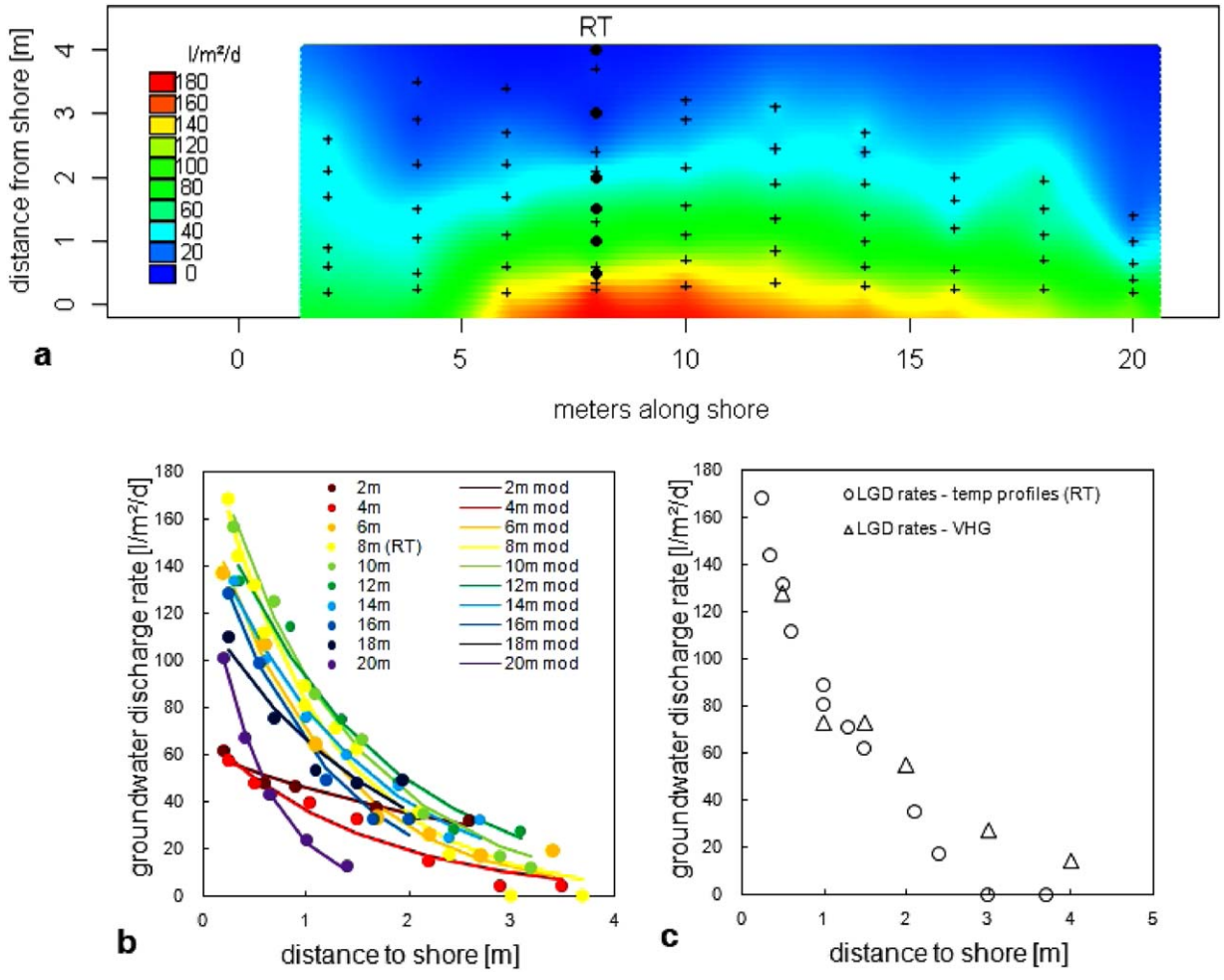

Figure 7. (a) Interpolated LGD rates in L m^{-2} d^{-1}; crosses mark locations of temperature depth profile measurements on which LGD rate calculations using the heat transport equation were based, black circles mark the location of piezometers. (b) LGD rates for all transects. Circles show values determined from temperature profiles with the heat transport equation, lines show LGD rates modeled with equation (5) as exponential decrease with distance to shore. (c) Comparison of LGD rates for the reference transect (RT) based on temperature profiles and VHGs.

between q_z estimates and $q_z(d_s)$ calculations (equation (5)) was minimal. As shown in Figure 7b, the estimates of $q_z(d_s)$ based on d_s matched the values for q_z estimated by fitting the heat transport equation quite well (RMSE: minimum 1.19 L m^{-2} d^{-1}, arithmetic mean 4.93 L m^{-2} d^{-1}, 90%-quantil 7.28 L m^{-2} d^{-1}, maximum 7.37 L m^{-2} d^{-1}, $n = 12$). Under the assumption that the exponential decrease of q_z defined by equation (5) can be extrapolated further offshore we calculated that for all except the most southern transect more than 70% of LGD occurred within the first 2 m and more than 90% within the first 4 m distance from the shore. For the most southern transect of the study site, 90% of LGD occurred within 8.4 m from the shore.

3.3. Fiber-Optic Distributed Temperature Sensing

[36] Temperature patterns obtained with DTS showed a general increase of lake bed surface temperature with distance to the shore (Figure 8). The lowest temperatures measured by FO-DTS were found in the midsection of the fiber-optic cable line closest to the shore. FO-DTS data covered a range of only 15.0–15.7°C, while profile temperatures closest to the surface at 4–8 cm depth ranged from 14.9 to 17.0°C. This discrepancy is possibly due to temperature fluctuations in the cold bath (which would be causing a general underestimation of temperatures) as well as a result of the fact that DTS measurements were carried out at noon, while most of the manual temperature measurements were carried out later in the day. However, these discrepancies are unlikely to affect our analyses (for more details see section 3.4). The fact that the range of the DTS temperatures is smaller than that of the manual measurements is discussed in section 4.3.

3.4. Upscaling Transect Measurements of LGD to the Shore Section

[37] DTS temperatures and LGD rates determined with depth profiles of sediment temperature were well correlated with a correlation coefficient of 0.87 for the entire shore section. A transfer function relating FO-DTS temperatures

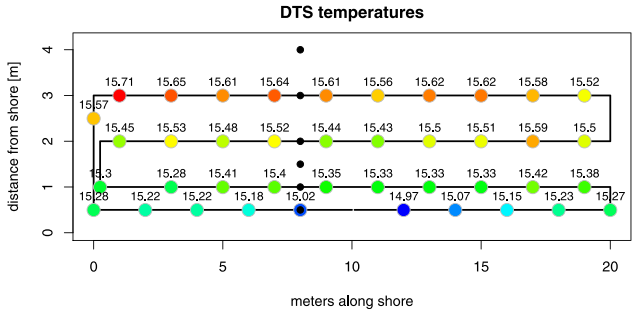

Figure 8. FO-DTS temperature data (2 m sampling resolution along the DTS cable).

to LGD rates determined with temperature depth profiles was derived based on a number of different setups from using the entire data set to using only four data pairs of FO-DTS temperatures and LGD rates at either of the transects A to D and at the reference transect (RT). As these transfer functions rely only on the patterns of DTS temperatures and their correlation with LGD rates a general shift in DTS temperatures due to possible underestimation will not affect model efficiency. Comparing linear models with exponential and quadratic transfer functions yielded that the exponential model produced consistently worse correlation coefficients and was therefore excluded from further analysis. In a next step, the linear and the quadratic models were evaluated in their performance and concerning the choice of calibration data set. It was found that the quadratic model did not produce better results than the simple linear model (even when using larger data sets than just one transect) (Figure 9 and Table 2). Given its simplicity we therefore chose the linear model as a transfer function of DTS temperatures to LGD rates. We furthermore found that the choice of transect influences the performance of the model (Table 2). Transect A seems to be the least suited transect for this type of analysis, likely because it covers both a smaller range of DTS temperatures as well as LGD rates. Transect B and the reference transect RT performed best among the transects. However, if we remove transect A from the comparison all linear transect models produce reasonable RMSE values. Median LGD rates can be overestimated by up to about 20% depending on choice of transect, mean and maximum LGD rates can also be slightly overestimated (generally less than 15%). The 50% model is generally just as good as the model using all data points for calibration (100% model). Both these models perform better than the models based on single transects alone. However, given their conservativeness in data needs the transect-based models perform surprisingly well and have the definite advantage of minimizing field effort. The performance measures for all models are summarized in Table 2. The lower left plot of Figure 9 shows the linear regressions of the five transect models and the lower mid plot the predicted values for the entire data set. The bad performance of transect model A becomes clear in a significant underprediction of LGD rates. The model based on the reference transect RT was chosen for further analysis and comparison as this transect is the only location where LGD rates from both VHG and temperature profiles are available. The transfer function resulting from the linear regression was ($R^2 = 0.92$):

$$\text{LGD-Rate}_{\text{Temp depth profile}} = 3429.1 - 219.2 * \text{FO-DTS temp} \quad (6)$$

[38] A similar regression analysis was carried out between the LGD rates derived from the VHGs at the same transect (Figure 7c) and resulted in the following transfer function ($R^2 = 0.998$):

$$\text{LGD-Rate}_{\text{VHG}} = 2618.3 - 166.0 * \text{FO-DTS temp} \quad (7)$$

[39] The third method employed to scale the transect measurements to the entire shore section was based on the simple exponential decline function fitted to the LGD rates determined with temperature depth profiles and does not make use of the FO-DTS measurements ($R^2 = 0.98$):

$$\text{LGD-Rate}_{\text{exponential decline}} = 205.2 * e^{(-0.895 * \text{distance to shore})} \quad (8)$$

[40] Results from all three upscaling methodologies were compared with the interpolated surface of LGD rates based on the entire grid of sediment temperature profiles (Figure 10). It was found that both upscaling methodologies based on FO-DTS data were able to reproduce the patterns of LGD. However, while the exponential decline function produces acceptable results along the main gradient (away from the shoreline), the lateral variability especially in close vicinity to the shore could only be reproduced by the DTS-based methodologies (Figure 10). This also becomes apparent when comparing the residuals between LGD rates from upscaling and based on temperature profiles (Figure 11). A comparison of RMSE, median and mean values for all three methodologies can be found in Table 2. The fact that several models also produce negative values does not suggest groundwater recharge at these locations but is due to the simple statistical relationship which is not bounded by zero.

4. Discussion

4.1. Estimation of LGD Rates

[41] The quantification of LGD rates based on temperature depth profiles or on VHGs is based on several assumptions:

[42] 1. It is a prerequisite that interpreted temperature differences are caused solely by the spatial variability of water fluxes and do not result from temporal variation of groundwater or surface water end-member temperatures. Since measurements were conducted in mid September on days where diurnal variation of air temperature did not exceed 6°C and as the investigation site is generally shaded by large beech trees, diurnal variations in surface water temperatures were assumed to be negligible and day to day variability of water temperature was only 1°C. Two small rainfall events occurred prior to the field measurements and could have introduced temporal dynamics to the head gradients at the site. As no pressure sensors were installed in the piezometers during this study, we have little information about the actual dynamics in gradients during these days. However, a piezometer installed at this location in

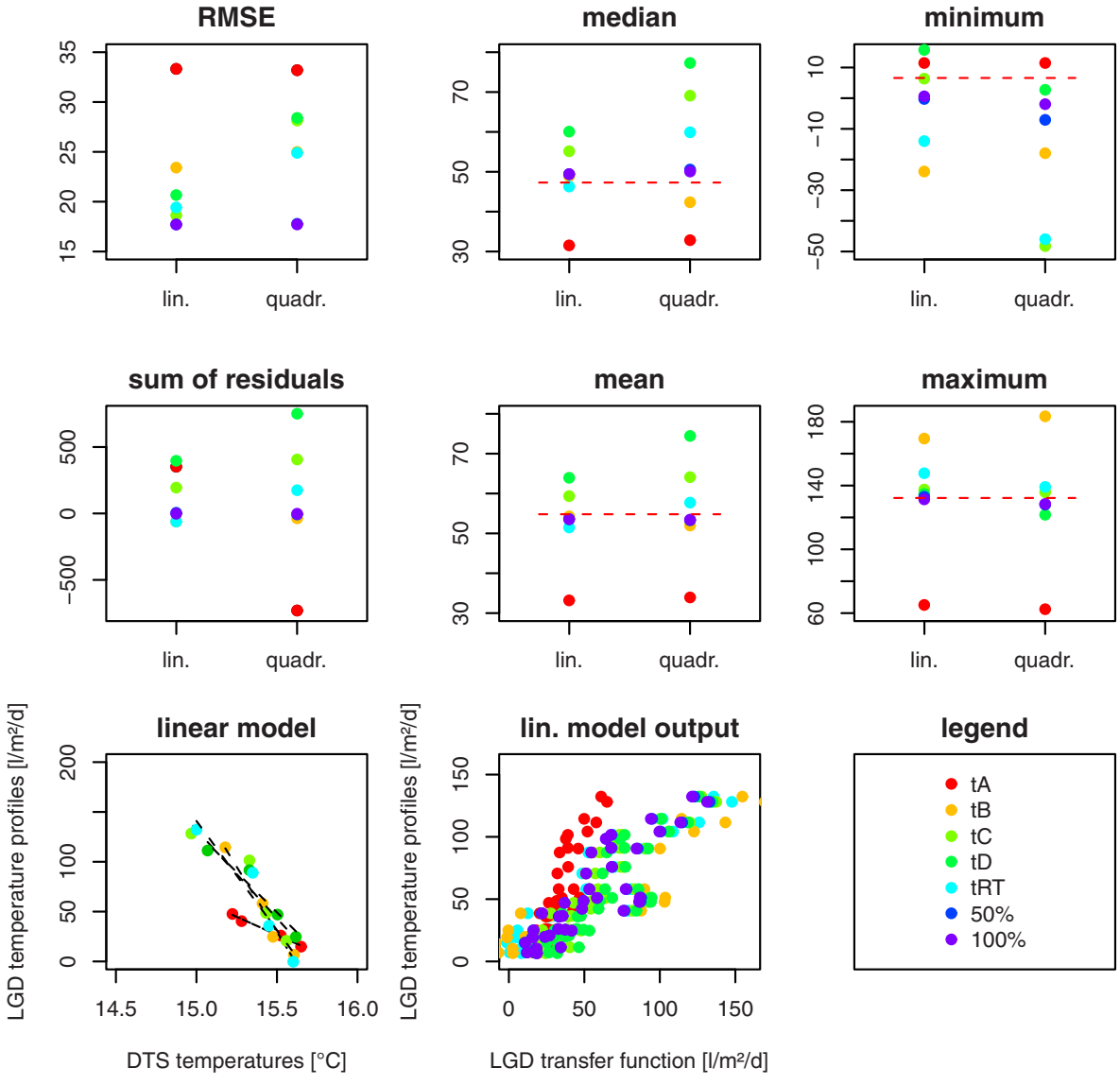

Figure 9. Evaluating model performance using the root mean square error (RMSE), the sum of residuals, and comparing the median, mean, minimum and maximum LGD rates of the predicted data set versus the LGD rates determined from the temperature profiles. This analysis was carried out for both linear and quadratic models based on different transects (transects A–D and the reference transect RT) as well as using every second value for calibration (50% model, $n = 21$) and the entire data set (100% model, $n = 41$). The red dashed lines show the corresponding "target values" of the temperature profile generated LGD rates. The two lower left plots show the linear regressions for the five transects models and the predicted values of LGD rates based on all linear transfer functions.

the following year was equipped with a pressure sensor (OTT Orpheus Mini, accuracy ±2 mm). Its rainfall response in October 2012 (similar sized rainfall events) was analyzed to estimate dynamics during our field campaign. It was found that the difference between piezometer and lake level had a very stable continuous baseline. Rainfall response resulted in small deviations (2–4 mm) from this baseline during the rainfall events and values very quickly returned to prior levels. Due to the quick recovery to baseline values we assume that our measurements are not strongly influenced by the dynamics in head gradients over the period when the measurements were taken. Repetition of several temperature profile measurements on consecutive days showed little change, which is another indication of quasi stable conditions during the measurement period. The fitting parameters a and b in equation (5) for the reference transect RT had similar values on both days: $a = 210.4$, $b = 0.887$ on the first day and $a = 196.3$, $b = 0.881$ on the second day. q_z values were also quite similar on both days, revealing a good reproducibility of the measurements. This implies that temporal variability of temperature and LGD rates was rather limited during the measurement campaign.

[43] 2. It is furthermore usually regarded as a necessary prerequisite that groundwater flow in the interface layer with a thickness L is exclusively vertical [e.g., *Schmidt*

Table 2. RMSE (Calculated Between Output of the Three Upscaling Methodologies at the DTS Sampling Locations and the Interpolated Surface of the Temperature Profile-Based LGD Rates), the Sum of the Residuals (as Measure of Bias) as Well as Mean, Median, and Range of LGD Rates

Upscaling Methodology	RMSE ($l/m^2/d$)	Sum of Residuals ($l/m^2/d$)	Median LGD ($l/m^2/d$)	Mean LGD ($l/m^2/d$)	Range of LGD ($l/m^2/d$)
From temperature profiles: Linear					
Transect A	33.3	353	31.5	33.2	11.5–65.1
Transect B	23.4	−63	48.1	54.3	−23.9–169.4
Transect C	18.7	192	55.2	59.4	6.3–137.5
Transect D	20.7	396	60.1	63.9	15.7–134.8
Ref. transect (RT)	19.4	−63	46.3	51.5	−14.0–147.8
50% of profiles	17.7	5	49.4	53.7	−0.2–132.9
100% of profiles	17.7	−1	49.4	53.5	0.7–131.3
Quadratic					
Transect A	33.17	−732	32.8	34	11.5–62.6
Transect B	24.98	−35	42.3	52	−17.9–183.3
Transect C	28.14	407	69.1	64.1	−48.3–135.9
Transect D	28.4	751	77.24	74.4	2.7–121.7
Ref. transect (RT)	24.9	174	59.9	57.7	−46–139.2
50% of profiles	17.77	−5.71	50.62	53.31	−7.1–128
100% of profiles	17.69	−2.33	50.06	53.47	−1.9–128.4
VHG based					
Ks (pump test)	20.1	−186	45.6	48.7	9.2–106.9
Ks (optimized)	19.2	260	57.0	60.9	11.3–133.8
Simplified					
Exponential function	27.5	396	34.3	64.7	14.0–131.2
LGD rates directly from temperature profiles	/	/	47.3	54.8	6.6–132.3

et al., 2006]. However, in fact it is only necessary that groundwater flow into the lake is parallel to all measurement points of the sediment temperature profile. In general, groundwater flow directions follow horizontal directions within the aquifer. Tracer tests [*Lee*, 1980] and modeling studies [e.g., *McBride and Pfannkuch*, 1975; *Pfannkuch and Winter*, 1984] have shown that upward curvature of flow paths occurs when groundwater approaches a lake. When applying the heat transport equation to calculate LGD rates, a flow path of length L has to be set which represents the flow in the transition zone in the lake sediment where groundwater temperatures approach lake temperatures (equation (3)). Traditionally, L is regarded as the thickness of the interface. However, if the extent of the temperature depth profile (here 0.45 m) is smaller than L (here 2 m) it is only required that vertical flow occurs in the uppermost 45 cm where measurements are conducted while more horizontal flow paths below 45 cm have no negative impact on the quality of the estimate. In our study, an optimum value of $L = 2$ m was found, however, another possible approach would have been to use L tending toward infinity, thus eliminating this parameter from the equation and further simplifying it, similar to the solution by *Turcotte and Schubert* [1982]. This solution was also used by *Schmidt et al*. [2007] and *Ferguson and Bense* [2011] and here applied to single-point measurements of temperature. Comparing the results of the two approaches did not produce significant differences for most of the data points (also found by *Ferguson and Bense* [2011]) and differed slightly for a few locations with very low fluxes.

[44] 3. Both, the hydraulic conductivity used in the calculation of LGD from VHG and the thermal conductivity used in the heat transport equation have not been determined directly (the first one having been estimated with a three different indirect methods and also through a single-pump test and the second one having been taken from the literature). It was found that if Ks was determined using grain size distributions, values were significantly higher than the values determined both with the pump test as well as by optimizing LGD to the LGD rates determined from the temperature profiles. The optimization of Ks results in a VHG transfer function which is not entirely independent of the temperature profile data set. For purposes of comparison, the pump test-based model was also included in Table 2.

[45] 4. The applied approach assumed that thermal and hydraulic properties of the lake bed were homogenous. This assumption introduces some uncertainty to the interpretation of the results of this study. As Ks values generally show a much stronger variability compared to thermal conductivities, relying on a single Ks value is likely to introduce more uncertainty than using a single value of thermal conductivity. However, from the 108 cm long sediment core taken at the site of the reference transect it is known that the sediment consisted of 94% sand and it can be assumed that thermal and hydraulic properties did not vary significantly with depth. The outwash plain sands surrounding the lake are generally quite uniform and also show little anisotropy, with a ratio of 1.02 (from 47 data pairs of vertical and horizontal Ks determined in soil cores extracted from the saturated zone during installation of observation wells in 2012—unpublished data). However, the fact that the lake sediment core did not reach the lower end of the interface and that its representative character for the entire field site was not tested, introduces further uncertainty into the interpretation of our results. Additional core samples or a higher number of piezometers and thus locations for pump tests would make it possible to test the assumption of relative homogeneity of the sediment and are subject of an ongoing study at the field site.

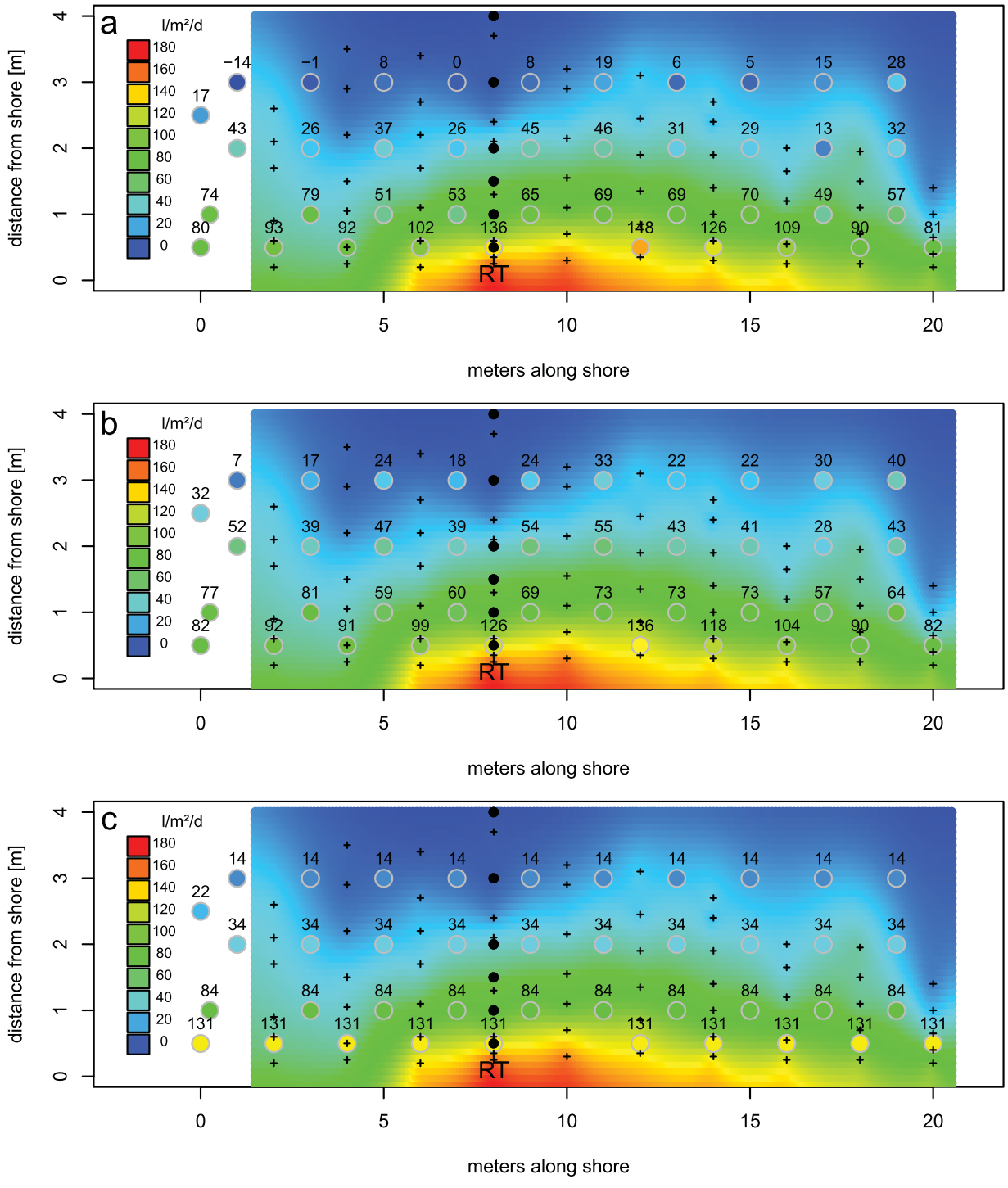

Figure 10. LGD rates determined with the three different upscaling methodologies. (a) Upscaling based on temperature profile transect, (b) upscaling based on VHG transect, (c) upscaling based on exponential function. The background colors depict the interpolated LGD rates from the sediment temperature profile grid. The circles and their corresponding numbers show the LGD rates determined with the upscaling methodologies at the sampling locations of the FO-DTS grid. The interpolated surface and the circle signatures are plotted using the same color scale.

[46] 5. The approaches based on temperatures are only applicable when groundwater and lake water temperatures differ significantly (i.e., in summer and winter) and will also fail at very high flow rates when the entire profile tends toward groundwater temperatures.

4.2. Concentration of Seepage in Nearshore Areas

[47] As previously reported by other authors in a homogeneous and isotropic aquifer, highest seepage rates occur usually close to the shore [*Pfannkuch and Winter*, 1984; *Belanger et al.*, 1985; *Shaw and Prepas*, 1990; *Schafran*

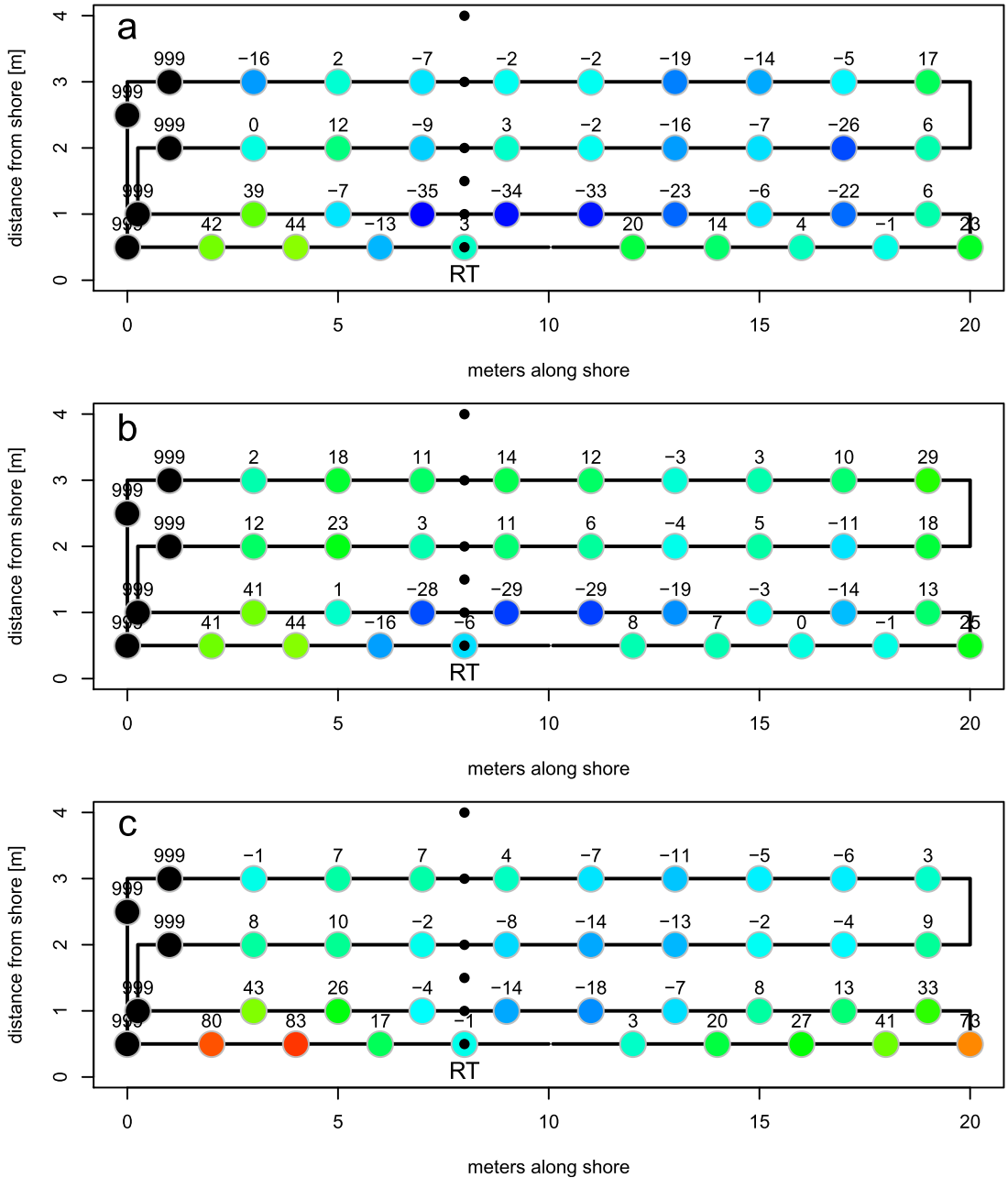

Figure 11. Residuals between LGD rates from the three upscaling methods and LGD rates based on temperature profiles. (a) Upscaling based on temperature profile transect, (b) upscaling based on VHG transect, (c) upscaling based on exponential function. Overestimations by the upscaling methodologies are shown as positive numbers. The color scale simply visualizes the corresponding values above the circles. 999 values correspond to no data values and indicate locations where DTS temperatures exist but no LGD data from temperature profiles is available for comparison.

and Driscoll, 1993; *Harvey et al*., 2000; *Kishel and Gerla*, 2002]. Similarly, our study also revealed that most seepage is focused in a very narrow band along the shore perimeter. For Lake Sallie, *McBride and* Pfannkuch [1975] report a decrease of 1 order of magnitude for every 60 m. In Lake Hinnensee, the observed nearshore decrease of LGD rates was even more intense (equation (5), Figure 7). Other authors also report exponential decrease of LGD rates [*Lee*, 1980; *Kishel and Gerla*, 2002].

4.3. Spatial Patterns of FO-DTS, VHGs, and Temperature Depth Profiles

[48] As mentioned above, patterns of groundwater inflow into the lake were found to be highly heterogeneous along the investigated shore section with large differences in the y direction (distance to shore) and smaller differences in the x direction (along the shore).

[49] All three methods were able to capture these patterns characterized by the strongly declining groundwater

Table 3. Evaluation of Three Methods for Their Usefulness in Capturing the Heterogeneity and Patterns of LGD

	Temperature Profiles	VHG	DTS
Capturing spatial variability and heterogeneity	Yes	Yes; even vertically if piezometer nests are used	Yes, but signals are smoothed out due to spatial averaging
Data accuracy	High	Medium	Strongly depending on effort of calibration
Estimation of LGD possible	Using heat transport equation	Using flow equation	Only through transfer function
Causes for uncertainties in determining LGD	Estimation of thermal characteristics; diurnal temperature variations; assumption of uniform characteristics; assumption of 1-D vertical flow	Estimation of hydraulic characteristics; assumption of uniform characteristics; assumption of 1-D vertical flow	Contact to sediment surface; dampening effects; calibration

influence with increasing distance to the shore. The reduced total range of temperatures determined by FO-DTS compared to the near-surface measurements of the temperature profiles can probably be attributed to two factors: (a) the fact that FO-DTS surveys averaged temperatures over the length of 4 m along the cable, which resulted in a smoothing of temperatures and (b) as the cable was deployed at the sediment surface the surface water temperature also had a dampening effect on the temperature patterns resulting from groundwater inflow. This dampening effect of surface temperature could be avoided if the fiber-optic cable was placed in the sediment instead of at the sediment surface [*Krause et al*., 2012]. However, special care would have to be taken to ensure a constant depth of deployment in the sediment over the entire length of the cable as temperatures are not only negatively correlated with groundwater discharge but also with sediment depth. It was found that VHGs determined at 50 cm depth (the depth closest to the measured temperature profiles) showed a weaker trend with distance to shore. This is most likely due to the large relative error and the relatively small differences in water level between lake and piezometer at this depth. As the relative error is smaller at 150 cm depth (larger differences in water level), the pattern emerges more clearly and therefore this data set was used for the transfer model. An evaluation of all three methods with respect to their potential in capturing LGD patterns on the one hand and main uncertainties on the other hand is summarized in Table 3.

[50] Besides the decrease of LGD with increasing distance to the shore, substantial heterogeneity of LGD rates has also been found along the shore. This spatial heterogeneity was indicated by the temperature depth profiles as well as FO-DTS. Large and small-scale stratigraphic heterogeneities and lake bed topographic structures can cause irregular LGD patterns. A decrease of LGD was observed at both ends of the study site (see Figures 7a and 10). At the northern end it was assumed that decreased LGD rates were caused by a concave bend of the shoreline so that a part of the groundwater flow paths approaching the shoreline are diverging. At the southern end of the study site reduced LGD rates were assumed to result from the impact of a large beech tree in close vicinity to the shore with some of its roots in the nearshore sediment. We assume that the free cross-sectional area for LGD is drastically reduced due to the dense root network. Furthermore, the reed stands observed in the same area have resulted in an accumulation of fine organic matter in the sediment, likely to be sealing fractions of the pore space and thus reducing the hydraulic conductivity. The impact of increased organic matter content at these locations might also be the reason for the overestimation of LGD rates by the FO-DTS data, as surface temperatures might be reduced due to differing thermal characteristics of this material.

4.4. Comparison of Upscaling Methodologies

[51] All three methods employed for upscaling measurements taken along a single transect to the entire shore section were able to reproduce the general pattern of heterogeneity, i.e., the strong decline of LGD with distance to shore described above (Figure 10). While the simple exponential decline function has the advantage of being low cost in both time and space it is intrinsically unable to reproduce the alongshore variability of LGD rates (Figure 10). On the other hand, upscaling approaches based on FO-DTS data sets are able to capture the spatial variability in both dimensions (Figure 10). However, the residuals for these methodologies are also quite high at both the northern and the southern end of the investigated shore section (Figure 11), indicating that the dampening of DTS temperatures due to (a) averaging and (b) the dampening effect of the surface water temperature, also dampens the variability of the upscaled LGD rates. The exponential decline upscaling approach overestimates LGD rates for the shore section, as the sum of the residuals is strongly positive and mean values are higher than for the "validation" data set (the LGD rates determined from the grid of temperature profiles) (Table 2). When comparing the two DTS-based approaches, the combination with the VHG transect seems to produce slightly better results; with RMSE of 19.2 $L/m^2/d$ compared to 19.4 $L/m^2/d$ of the temperature profile—DTS combination (linear model RT Table 2). However, for the VHG-DTS combination both median and mean values are higher than the LGD rates determined with the temperature profile—DTS combination and also compared to the rates of the validation data set (Table 2). RMSE values for the exponential decline-based upscaling are significantly higher with 27.5 $L/m^2/d$; furthermore, median values are low and mean values are high compared to all other data sets, indicating a generally different frequency distribution. LGD rates appear to be slightly underestimated by the temperature profile-DTS-based methodology as the sum of residuals has a negative value (Table 2), in contrast to the strongly positive values of the other two upscaling approaches. Taking all evaluation measures into account, the temperature profile-DTS

combination proves to be the most promising with mean and median LGD rates close to those of the validation data set, low bias, and low RMSE. The DTS-based approach can here be used only to estimate LGD rates, water fluxes from lake to groundwater cannot be determined. As a result, zero flux will be estimated also for locations of groundwater recharge. All methodologies assume 1-D vertical flow and homogeneous sediment, concerning both its hydraulic as well as thermal characteristics. This simplification seems viable along the studied shore section but might not hold for larger scale applications. In this case, sediment variability will need to be included in the upscaling approach.

5. Conclusions

[52] The determination of water fluxes between groundwater and surface water is a major challenge due to strong spatial variability and the need of integrating measurements at various scales. Therefore, the combination of methods tested within the present study, combining FO-DTS with methods for spot quantifications of seepage rates (in this case temperature depth profiles and vertical hydraulic gradients) proved to be a successful upscaling approach. The DTS-based upscaling approaches reliably reproduced 2-D patterns of lacustrine groundwater discharge rates using only four data points of either VHG- or sediment temperature profile determined LGD rates and the DTS temperature grid. The proof of concept and of reliability of FO-DTS applications for quantifying spatial patterns of exchange fluxes across aquifer-lake interfaces that are provided in this study encourage the extension of investigations to larger scales.

[53] **Acknowledgments.** Fieldwork was carried out in the TERENO observatory of north-east Germany, which is funded by the Helmholtz Association. The authors would like to thank Scott Tyler and two anonymous reviewers for their very useful comments and suggestions, which helped in improving the paper considerably; furthermore Knut Günther and Kathleen Rathenow for their help during the field campaign, and Janek Dreibrodt, Christina Tecklenburg, and Henriette Wilke for their help with sediment characterization and the Mueritz National Park Authorities for their cooperation.

References

Anibas, C., J. H. Fleckenstein, N. Volze, K. Buis, R. Verhoeven, P. Meire, and O. Batelaan (2009), Transient or steady-state? Using vertical temperature profiles to quantify groundwater-surface water exchange, *Hydrol. Processes*, *23*(15), 2165–2177.

Belanger, T. V., D. F. Mikutel, and P. A. Churchill (1985), Groundwater seepage nutrient loading in a Florida lake, *Water. Res.*, *19*(6), 773–781.

Bredehoeft, J. D., and I. S. Papadopulos (1965), Rates of vertical groundwater movement estimated from Earth's thermal profile, *Water. Resour. Res.*, *1*(2), 325–328.

Brock, T. D., D. R. Lee, D. Janes and D. Winek (1982), Groundwater seepage as a nutrient source to a drainage lake—Lake Mendota, Wisconsin, *Water. Res.*, *16*(7), 1255–1263.

Cherkauer, D. S., and D. C. Nader (1989), Distribution of groundwater seepage to large surface-water bodies: The effect of hydraulic heterogeneities, *J. Hydrol.*, *109*, 151–165.

Constanz, J. (2008), Heat as a tracer to determine streambed water exchanges, *Water. Resour. Res.*, *44*, W00D10, doi:10.1029/2008WR006996.

Enell, M. (1982), The phosphorus economy of a hypertrophic seepage lake in Scania, south Sweden: Groundwater influence, *Hydrobiologia*, *86*(1–2), 153–158.

Ferguson, G., and V. Bense (2011), Uncertainty in 1D heat-flow analysis to estimate groundwater discharge to a stream, *Groundwater*, *49*(3), 336–347.

Frape, S. K., and R. J. Patterson (1981), Chemistry of interstitial water and bottom sediments as indicators of seepage patterns in Perch Lake, Chalk-River, Ontario, *Limnol. Oceanogr.*, *26*(3), 500–517.

Hannah, D. M., I. A. Malcolm, and C. Bradley (2009), Seasonal hyporheic temperature dynamics over riffle bedforms, *Hydrol. Processes*, *23*(15), 2178–2194, doi: 10:1002/hyp.7256.

Harvey, F. E., D. L. Rudolph, and S. K. Frape (2000), Estimating ground water flux into large lakes: Application in the Hamilton Harbor, western Lake Ontario, *Ground Water*, *38*(4), 550–565.

Hatch, C. E., A. T. Fisher, J. S. Revenaugh, J. Constantz, and C. Ruehl (2006), Quantifying surface water–groundwater interactions using time series analysis of streambed thermal records: Method development, *Water Resour. Res.*, *42*, W10410, doi.10.1029/2005WR004787.

Hausner, M. B., F. Suárez, K. E. Glander, N. van de Giesen, J. S. Selker, and S. W. Tyler (2011), Calibrating single-ended fiber-optic Raman spectra distributed temperature sensing data, *Sensors*, *11*, 10,859–10,879.

Henderson, R. D., F. D. Day-Lewis, and C. F. Harvey (2009), Investigation of aquifer-estuary interaction using wavelet analysis of fiber-optic temperature data, *Geophys. Res. Lett.*, *36*, L06403, doi:10.1029/2008GL036926.

Jensen, J. K., and P. Engesgaard (2011), Nonuniform groundwater discharge across a streambed: Heat as a tracer, *Vadose Zone J.*, *10*, 98–109, doi:10.2136/vzj2010.0005.

Kaeser, D., A. Binley, L. Heathwaite, and S. Krause (2009), Spatio-temporal variations of hyporheic flow in a riffle-step-pool sequence, *Hydrol. Processes*, *23*(15), 2138–2149, doi:10.1002/hyp.7317.

Kalbus, E., F. Reinstorf, and M. Schirmer (2006), Measuring methods for groundwater—Surface water interactions: A review, *Hydrol. Earth Syst. Sci.*, *10*(6), 873–887.

Kidmose, J., P. Engesgaad, B. Nilsson, T. Laier, and M. C. Looms (2011), Spatial distribution of seepage at a flow-through lake: Lake Hampen, Western Denmark, *Vadose Zone J.*, *10*, 110–124, doi: 10.2136/vzj.2010.0017.

Kishel, H. F., and P. J. Gerla (2002), Characteristics of preferential flow and groundwater discharge to Shingobee Lake, Minnesota, USA, *Hydrol. Processes*, *16*(10), 1921–1934.

Krabbenhoft, D. P., and K. E. Webster (1995), Transient hydrogeological controls on the chemistry of a seepage lake, *Water. Resour. Res.*, *31*(9), 2295–2305.

Krabbenhoft, D. P., C. J. Bowser, M. P. Anderson, and J. W. Valley (1990a), Estimating groundwater exchange with lakes: 1. The stable isotope mass balance method, *Water. Resour. Res.*, *26*(10), 2445–2453.

Krabbenhoft, D. P., M. P. Anderson, and C. J. Bowser (1990b), Estimating groundwater exchange with lakes: 2. Calibration of a 3-dimensional solute transport model to a stable isotope plume, *Water. Resour. Res.*, *26*(10), 2455–2462.

Krabbenhoft, D. P., C. J. Bowser, C. Kendall, and J. R. Gat (1994), Use of O-18 and deuterium to assess the hydrology of groundwater-lake systems, *Environ. Chem. Lakes Reservoirs*, *237*, 67–90.

Krause, S., A. L. Heathwaite, A. Binley, and P. Keenan (2009), Nitrate concentration changes along the groundwater—Surface water interface of a small Cumbrian river, *Hydrol. Processes*, *23*(15), 2195–2211.

Krause, S., D. M. Hannah, and T. Blume (2011), Heat transport patterns at pool-riffle sequences of an UK lowland stream, *Ecohydrol. J.*, *4*(4), 549–563, doi:10.1002/eco.199.

Krause, S., T. Blume, and N. J. Cassidy (2012), Investigating patterns and controls of groundwater up-welling in a lowland river by combining fibre-optic distributed temperature sensing with observations of vertical head gradients, *Hydrol. Earth Syst. Sci.*, *16*, 1775–1792.

Lautz, L. K., and R. E. Ribaudo (2012), Scaling up point-in-space heat tracing of seepage flux using bed temperatures as a quantitative proxy, *Hydrogeol. J.*, *20*, 1223–1238.

Lee, D. R. (1977), Device for measuring seepage flux in lakes and estuaries, *Limnol. Oceanogr.*, *22*(1), 140–147.

Lee, D. R. (1980), Groundwater—Solute influx, *Limnol. Oceanogr.*, *25*(1), 183–186.

Loeb, S. L., and C. R. Goldman (1979), Water and nutrient transport via groundwater from Ward Valley into Lake Tahoe, *Limnol. Oceanogr.*, *24*(6),1146–1154.

Lowry, C. S., J. F. Walker, R. J. Hunt, and M. P. Anderson (2007), Identifying spatial variability of groundwater discharge in a wetland stream using

a distributed temperature sensor, *Water Resour. Res.*, *43*, W10408, doi:10.1029/2007WR006145.

McBride, M. S., and H. O. Pfannkuch (1975), Distribution of seepage within lakebeds, *J. Res. U.S. Geol. Surv.*, *3*(5), 505–512.

Meinikmann, K., G. Nützmann, and J. Lewandowski (2013), Lacustrine groundwater discharge: Combined determination of volumes and spatial patterns, *J. Hydrol.*, *502*, 202–211.

Mortimer, R. J. G., M. D. Krom, D. R. Boyle, and A. Nishri (1999), Use of a high-resolution pore-water gel profiler to measure groundwater fluxes at an underwater saline seepage site in Lake Kinneret, Israel, *Limnol. Oceanogr.*, *44*(7), 1802–1809.

Mwakanyamale, K., L. Slater, F. Day-Lewis, M. Elwaseif, and C. Johnson (2012), Spatially variable stage-driven groundwater-surface water interaction inferred from time-frequency analysis of distributed temperature sensing data, *Geophys. Res. Lett.*, *39*, L06401, doi:10.1029/2011GL050824.

Pfannkuch, H. O., and T. C. Winter (1984), Effect of anisotropy and groundwater system geometry on seepage through lakebeds: 1. Analog and dimensional analysis, *J. Hydrol.*, *75*(1–4), 213–237.

Rosenberry, D. O. (2005), Integrating seepage heterogeneity with the use of ganged seepage meters, *Limnol. Oceanogr. Methods*, *3*, 131–142.

Schafran, G. C., and C. T. Driscoll (1993), Flow path composition relationships for groundwater entering an acidic lake, *Water. Resour. Res.*, *29*(1), 145–154.

Schmidt, C., M. Bayer-Raich, and M. Schirmer (2006), Characterization of spatial heterogeneity of groundwater-stream water interactions using multiple depth streambed temperature measurements at the reach scale, *Hydrol. Earth Syst. Sci.*, *10*, 849–859.

Schmidt, C., B. Conant, M. Bayer-Raich, and M. Schirmer (2007), Evaluation and field-scale application of an analytical method to quantify groundwater discharge using mapped streambed temperatures, *J. Hydrol.*, *347*(3–4), 292–302.

Schuster, P. F., M. M. Reddy, J. W. LaBaugh, R. S. Parkhurst, D. O. Rosenberry, T. C. Winter, R. C. Antweiler, and W. E. Dean (2003), Characterization of lake water and ground water movement in the littoral zone of Williams Lake, a closed-basin lake in north central Minnesota, *Hydrol. Processes*, *17*(4), 823–838.

Selker, J. S., L. Thévanaz, H. Huwald, A. Mallet, W. Luxemburg, N. van de Giesen, M. Stejskal, J. Zeman, M. C. Westhoff, and M. B. Parlange (2006a), Distributed fiber-optic temperature sensing for hydrologic systems, *Water Resour. Res.*, *42*, W12202, doi:10.1029/2006WR005326.

Selker, J. S., N. C. van de Giesen, M. Westhoff, W. Luxemburg, and M. Parlange (2006b), Fiber-optics opens window on stream dynamics, *Geophys. Res. Lett.*, *33*, L24401, doi:10.1029/2006GL027979.

Sensornet (2009), *Sentinal DTS User Guide SEN2-UM1.0*, London, U. K.

Shaw, R. D., and E. E. Prepas (1990), Groundwater lake interactions. 2. Nearshore seepage patterns and the contribution of ground-water to lakes in Central Alberta, *J. Hydrol.*, *119*(1–4), 121–136.

Shaw, R. D., J. F. H. Shaw, H. Fricker, and E. E. Prepas (1990), An integrated approach to quantify groundwater transport of phosphorus to Narrow Lake, Alberta, *Limnol. Oceanogr.*, *35*(4), 870–886.

Slater, L. D., D. Ntarlagiannis, F. D. Day-Lewis, K. Mwakanyamale, R. J. Versteeg, A. Ward, C. Strickland, C. D. Johnson, and J. W. Lane Jr. (2010), Use of electrical imaging and distributed temperature sensing methods to characterize surface water–groundwater exchange regulating uranium transport at the Hanford 300 Area Washington, *Water Resour. Res.*, *46*, W10533, doi:10.1029/2010WR009110.

Stauffer, R. E. (1985), Use of solute tracers released by weathering to estimate groundwater inflow to seepage lakes, *Environ. Sci. Technol.*, *19*(5), 405–411.

Stonestrom, D. A., and J. Constantz (2003), Heat as a tool for studying the movement of ground water near streams, *U.S. Geol. Surv. Circ.* 1260, Reston, Va.

Turcotte, D., and G. Schubert (1982), Geodynamics: Application of Continuum Physics to Geological Problems, John Wiley, New York.

Tyler, S. W., J. S. Selker, M. B. Hausner, C. E. Hatch, T. Torgersen, C. E. Thodal, and S. G. Schladow (2009), Environmental temperature sensing using Raman spectra DTS fiber-optic methods, *Water Resour. Res.*, *45*, W00D23, doi:10.1029/2008WR007052.

Van de Giesen, N., S. C. Steele-Dunne, J. Jansen, O. Hoes, M. B. Hausner, S. Tyler, and J. Selker (2012), ''Double-ended calibration of fiber-optic Raman spectra distributed temperature sensing data'', *Sensors*, *12*(5), 5471–5485.